

Theoretical study of resonance modes of coupled thin films in the rigid layer model

A. Layadi

Departement de Physique, Université Ferhat Abbas, Sétif 19000, Algeria

(Received 19 November 2003; published 30 April 2004)

An investigation of the ferromagnetic resonance (FMR) modes is done for a two coupled ferromagnetic film system in the framework of the rigid layer model. In this case, one of the layers (the driver layer) has a strong in-plane anisotropy compared to the coupling strength and to in-plane anisotropy of the other layer (the sensor). The curves of dispersion relation, the resonant frequency f , and the mode intensity I vs applied field H are discussed as a function of the bilinear J_1 and biquadratic J_2 coupling terms, and of the angle δ between the in-plane uniaxial anisotropy easy axis directions in the two layers. Depending on the coupling strength and δ values and the anisotropy of the sensor layer, as the applied field is increased, the sensor layer magnetization may smoothly rotate or suddenly switch from the antiparallel configuration to the saturated state. In the latter case, a discontinuity is observed in the mode position as well as in the FMR intensity. The discontinuities are more important for the optical than for the acoustic modes. Moreover, the coupling strengths (J_1, J_2) affect the mode intensity but, practically, not the position of the acoustic mode; while for the optical mode, the effect of these parameters on the f vs H and I vs H curves is more apparent. Also, for all δ angles (other than 0 and 90°), no effect of δ is observed on the position and intensity of the high-frequency mode but δ does affect the lower-frequency mode position.

DOI: 10.1103/PhysRevB.69.144431

PACS number(s): 76.50.+g, 76.20.+q, 75.70.Cn, 75.30.Gw

I. INTRODUCTION

A system of two coupled layers separated by a nonmagnetic interlayer has been intensively studied in the last decade.¹ Several theoretical models have been proposed to explain certain experimental observations; the bilinear coupling² J_1 , the biquadratic coupling³⁻⁹ J_2 (and even higher-order coupling terms¹⁰) and different magnetocrystalline anisotropies¹¹⁻¹⁹ were considered. In the rigid layer model (rigid driver model¹¹), one layer (the driver) has a very strong in-plane anisotropy compared to the coupling strength (the weak coupling case) and to the anisotropy of the second layer (the sensor layer). In this situation, if a magnetic field, applied along the easy axis of the driver layer, is decreased, it can be assumed that the driver layer magnetization remains along the easy axis (for all H values), while the sensor layer magnetization may rotate away from the applied field direction under its own in-plane anisotropy (if the easy axis is not parallel to that of the driver layer), a negative J_1 coupling parameter which tends to antiferromagnetically align the magnetizations or a negative J_2 value which favors a perpendicular configuration of the magnetizations, i.e., a 90°-type coupling. Elmers *et al.*¹¹ considered layers with orthogonal in-plane anisotropy axes and, by using magnetization curves (based on the magneto-optical Kerr effect), they showed that, in the framework of this model, one can derive separate values of J_1 and J_2 .

Ferromagnetic resonance (FMR) has been widely used to study the magnetic coupling in multilayers.^{10,12-22} In the present work, a description of the FMR modes will be given in the rigid layer model situation, with two layers characterized by in-plane anisotropy whose easy axes make an arbitrary angle δ between them; the orthogonal anisotropy case, worked out by Elmers *et al.*,¹¹ will be illustrated as particular example ($\delta=90^\circ$). In Sec. II, the layer configurations and the system energy will be outlined; detailed calculations, in

the more general case, for the resonance frequency and mode intensity relations are given elsewhere.^{13,14} Equilibrium relations pertaining to the rigid model case will be worked out and discussed in Sec. III. In Sec. IV, the dispersion relation is studied, and the resonance frequency and the FMR intensity are discussed as functions of the applied field H and of the coupling strengths J_1 and J_2 in the framework of the rigid layer model.

II. PRELIMINARY CONSIDERATIONS

The system considered here has been described elsewhere^{13,14} in the more general case. Following is an outline of the system configuration and a description of the different terms in the total energy. It is assumed that the two thin film layers, denoted as A and B , lie in the x - y plane, with the z axis normal to the film plane. They are coupled to each other through a nonmagnetic layer. The magnetization \mathbf{M}_A of layer A is defined, in spherical coordinates, by the angles θ_A and ϕ_A ; and similarly \mathbf{M}_B (layer B) by the angles θ_B and ϕ_B . The layers are supposed to have in-plane uniaxial magnetocrystalline anisotropies. For layer A , the easy axis of such an anisotropy is taken to be along the x axis; the corresponding energy will then be $E_{A \text{ in}} = -K_A \sin^2 \theta_A \cos^2 \phi_A$. For layer B , the easy axis has an arbitrary direction within the plane it makes an angle δ with the x axis; following the analysis in Ref. 16, the magnetocrystalline energy can be written as $E_{B \text{ in}} = -K_B \sin^2 \theta_B \cos^2(\phi_B - \delta)$. K_A (K_B) is the in-plane magnetocrystalline anisotropy constant for layer A (layer B); K_A and K_B are positive since it is assumed that the anisotropy axes are easy directions. The external applied magnetic field \mathbf{H} is taken to be in the plane of the films, making an angle α with the x axis. The microwave field \mathbf{h} is along the y axis. With all these considerations, the total free energy of the system per unit area can be explicitly written as^{13,14}

$$\begin{aligned}
E = & t_A \{ -M_A H \sin \theta_A \cos(\alpha - \varphi_A) + K_{u \text{ eff } A} \sin^2 \theta_A \\
& - K_A \sin^2 \theta_A \cos^2 \varphi_A \} + t_B \{ -M_B H \sin \theta_B \cos(\alpha - \varphi_B) \\
& + K_{u \text{ eff } B} \sin^2 \theta_B - K_B \sin^2 \theta_B \cos^2(\varphi_B - \delta) \} \\
& - J_1 \{ \sin \theta_A \sin \theta_B \cos(\varphi_A - \varphi_B) + \cos \theta_A \cos \theta_B \} \\
& - J_2 \{ \sin \theta_A \sin \theta_B \cos(\varphi_A - \varphi_B) + \cos \theta_A \cos \theta_B \}^2. \quad (1)
\end{aligned}$$

In the two first terms of Eq. (1), t_A and t_B are the thicknesses of layers A and B , respectively. The total energy E consists for layer A (the first term) of the Zeeman energy (interaction of the external magnetic field \mathbf{H} with the magnetizations) $-M_A H \sin \theta_A \cos(\alpha - \varphi_A)$, the shape, and any out-of-plane uniaxial anisotropy given by the constant $K_{u \text{ eff } A}$ where $K_{u \text{ eff } A} = K_{uA} - 2\pi M_A^2$, K_{uA} is the out-of-plane magnetocrystalline anisotropy constant for layer A , and the in-plane magnetocrystalline anisotropy. For layer B [the second term in Eq. (1)], the above relations hold by changing the subscript A to B and adding the in-plane anisotropy (written above). The interlayer coupling energy is given by the two last terms. J_1 and J_2 are, respectively, the bilinear and biquadratic coupling parameters. The nature and the strength of the coupling are described by the sign and the magnitude of J_1 and J_2 . When J_1 dominates and if it is positive, the energy is minimal when \mathbf{M}_A and \mathbf{M}_B are parallel (ferromagnetic coupling), while if it is negative, then the lowest energy is achieved when \mathbf{M}_A and \mathbf{M}_B are antiparallel (antiferromagnetic coupling). If, on the other hand J_2 dominates and is negative (which was experimentally observed), then the minimum energy occurs when the magnetizations are oriented perpendicular to each other (the 90° -type coupling¹). Note also that this coupling analysis is a phenomenological one, with no assumption made about the origin of the coupling. The bilinear coupling is believed to be due to the Ruderman-Kittel-Kasuya-Yosida (RKKY) interaction, mainly in transition metals, since this interaction can be written as a scalar product of the magnetizations.¹ The biquadratic coupling could arise from a variation of the interlayer thickness.⁵ Note that, at equilibrium, the magnetizations \mathbf{M}_A and \mathbf{M}_B must lie in the film plane, i.e., $\theta_A = \theta_B = 90^\circ$, due to the strong demagnetizing field of the thin films and to the fact that the applied magnetic field is in plane.

The angles $\varphi_{A,B}$ are given by the following two coupled equations (the equilibrium conditions):

$$\begin{aligned}
H \sin(\alpha - \varphi_A) = & \frac{1}{2} H_{KA} \sin 2\varphi_A + \frac{J_1}{t_A M_A} \sin(\varphi_A - \varphi_B) \\
& + \frac{J_2}{t_A M_A} \sin 2(\varphi_A - \varphi_B) \quad (2a)
\end{aligned}$$

and

$$\begin{aligned}
H \sin(\alpha - \varphi_B) = & \frac{1}{2} H_{KB} \sin 2(\varphi_B - \delta) - \frac{J_1}{t_B M_B} \sin(\varphi_A - \varphi_B) \\
& - \frac{J_2}{t_B M_B} \sin 2(\varphi_A - \varphi_B), \quad (2b)
\end{aligned}$$

where $H_{KA} = 2K_A/M_A$ ($H_{KB} = 2K_B/M_B$) is the planar anisotropy field for layer A (layer B).

III. THE RIGID LAYER MODEL

In the rigid layer model (rigid driver model¹¹), one of the layers (here, layer A) has a very strong in-plane magnetocrystalline anisotropy (with the easy axis taken to be along the x axis) compared to that of the second layer (layer B) (with the easy axis making an angle δ with the x axis) and to the coupling strength, i.e., $H_{KA} \gg H_{KB}, J_1/t_A M_A, J_2/t_A M_A$. In this case it can be assumed that if an applied magnetic field along the x axis is decreased, the magnetization \mathbf{M}_A will always remain along the layer A easy axis (the x axis), i.e., $\varphi_A = 0^\circ$ for all H values. On the other hand, as H is decreased, \mathbf{M}_B might move away from the field direction under the effect of (i) layer B in-plane anisotropy (if the layer B easy direction is not along the x axis, i.e., $\delta \neq 0^\circ$), (ii) a negative bilinear J_1 coupling parameter which tends to make \mathbf{M}_A and \mathbf{M}_B antiparallel, and (iii) a negative biquadratic coupling J_2 value which favors the perpendicular configuration of the magnetizations, i.e., a 90° -type coupling. The \mathbf{M}_B direction will then be given by the competition of these three phenomena. Putting $\varphi_A = 0^\circ$ in Eqs. (2a) and (2b) and making the appropriate approximations (mentioned above), the φ_B angle will be the solution of the following equation, for an arbitrary δ value:

$$\begin{aligned}
H \sin \varphi_B + \frac{1}{2} H_{KB} \sin 2(\varphi_B - \delta) + \frac{J_1}{t_B M_B} \sin \varphi_B \\
+ \frac{J_2}{t_B M_B} \sin 2\varphi_B = 0. \quad (3)
\end{aligned}$$

For the most studied situation where the easy axes in the two layers are parallel ($\delta = 0^\circ$), the solution of Eq. (3) will be as follows:

$$\varphi_B = 0^\circ \quad \text{if } H > H_{\text{sat}}(\delta = 0^\circ), \quad (4a)$$

$$\begin{aligned}
\cos \varphi_B = - \frac{t_B M_B H + J_1}{t_B M_B H_{KB} + 2J_2} \\
\text{for } H_{\text{crit}}(\delta = 0^\circ) < H < H_{\text{sat}}(\delta = 0^\circ), \quad (4b)
\end{aligned}$$

$$\varphi_B = 180^\circ \quad \text{if } H < H_{\text{crit}}(\delta = 0^\circ). \quad (4c)$$

For perpendicular easy axes, i.e., $\delta = 90^\circ$,

$$\varphi_B = 0^\circ \quad \text{if } H > H_{\text{sat}}(\delta = 90^\circ), \quad (5a)$$

$$\begin{aligned}
\cos \varphi_B = \frac{t_B M_B H + J_1}{t_B M_B H_{KB} - 2J_2} \\
\text{for } H_{\text{crit}}(\delta = 90^\circ) < H < H_{\text{sat}}(\delta = 90^\circ), \quad (5b)
\end{aligned}$$

and

$$\varphi_B = 180^\circ \quad \text{if } H < H_{\text{crit}}(\delta = 90^\circ). \quad (5c)$$

Here $H_{\text{sat}}(\delta)$ denotes the saturation field, the field above which the magnetizations are parallel, along the applied field H direction; $H_{\text{crit}}(\delta)$ is the critical field, i.e., the field under which the magnetizations become antiparallel under a negative J_1 . $H_{\text{sat}}(\delta)$ and $H_{\text{crit}}(\delta)$ are found by minimizing the

total energy and making the approximation pertaining to the rigid layer model. These fields are found to be

$$H_{\text{sat}}(\delta) = -\frac{J_1 + 2J_2}{t_B M_B} - H_{KB} \cos 2\delta \quad (6)$$

and

$$H_{\text{crit}}(\delta) = -\frac{J_1 - 2J_2}{t_B M_B} + H_{KB} \cos 2\delta. \quad (7)$$

Two remarks should be made about these relations. First, Eqs. (4a)–(7) are valid only for $\delta=0^\circ$ (parallel easy axes) and $\delta=90^\circ$ (orthogonal easy axes); for other δ values, \mathbf{M}_B will asymptotically align along \mathbf{H} (asymptotic saturation) for a strong H value and also \mathbf{M}_B will asymptotically reach the $\phi_B=180^\circ$ direction when the effect of a negative J_1 will overcome the effect of H ; this is because $\phi_B=0^\circ$ and $\phi_B=180^\circ$ are not exact solutions of Eq. (3) for arbitrary δ . Second, $H_{\text{crit}}(\delta)$ is defined only for antiferromagnetic coupling ($J_1 < 0$) where \mathbf{M}_A and \mathbf{M}_B might be antiparallel; assuming $t_A M_A > t_B M_B$, \mathbf{M}_A will be along \mathbf{H} while \mathbf{M}_B is opposite to it. For ferromagnetic coupling ($J_1 > 0$), the solution $\phi_B=180^\circ$, in Eqs. (4c) and (5c), does not hold and the inequalities in Eqs. (4b) and (5b) must be changed to $H < H_{\text{sat}}(\delta)$.

For this antiferromagnetic coupling, H_{sat} and H_{crit} can be inferred, for instance, from FMR, through the dispersion relation, as will be seen in the next section. From the knowledge of H_{sat} and H_{crit} , the coupling strength parameters J_1 and J_2 can be independently determined. Indeed, it is easy to see from Eqs. (6) and (7) that

$$J_1 = -\frac{t_B M_B}{2} (H_{\text{sat}} + H_{\text{crit}}). \quad (8)$$

Equation (8) is valid for $\delta=0^\circ$ as well as $\delta=90^\circ$. The bi-quadratic coupling J_2 is found to be

$$J_2 = -\frac{t_B M_B}{4} (\pm 2H_{KB} + H_{\text{sat}} - H_{\text{crit}}) \quad (9)$$

where the $+$ ($-$) sign corresponds to $\delta=0^\circ$ ($\delta=90^\circ$). Recall that these relations are valid in the rigid layer model only.

IV. THE FMR MODE POSITION AND INTENSITY

The equation giving the normal modes (resonance frequency) of such a system in the more general case as well as the FMR intensity relation have been derived in Ref. 13. Recall that the resonance frequency (with a fixed dc field set up) is given by the following fourth-order equation in ω (the resonant frequency):¹³

$$\begin{aligned} & \left[\frac{ab}{\gamma_A \gamma_B} \right]^2 \omega^4 - \left[a^2 b^2 \left(\frac{H_1^A H_2^A}{\gamma_B^2} + \frac{H_1^B H_2^B}{\gamma_A^2} \right) + abc_1 \left(\frac{aH_2^B}{\gamma_A} \right. \right. \\ & \left. \left. + \frac{bH_2^A}{\gamma_B} \right) + abc_2 \left(\frac{aH_1^B}{\gamma_A} + \frac{bH_1^A}{\gamma_B} \right) + c_1 c_2 \left(\frac{a^2}{\gamma_A^2} + \frac{b^2}{\gamma_B^2} \right) \right. \\ & \left. + \frac{2c_0 c_2 ab}{\gamma_A \gamma_B} \right] \omega^2 + [abH_2^A H_2^B + c_2 (aH_2^A + bH_2^B)] \\ & \times [abH_1^A H_1^B + c_1 (aH_1^A + bH_1^B) + (c_1^2 - c_0^2)] = 0. \quad (10) \end{aligned}$$

Here $a = t_A M_A$, $b = t_B M_B$, γ_A and γ_B denote the gyromagnetic ratios of layers A and B, respectively. In the present particular case $\alpha=0^\circ$ (\mathbf{H} along the x axis) and with the rigid layer approximation ($\phi_A=0^\circ$), the different quantities entering Eq. (10) are as follows: $c_0 = J_1 + 2J_2 \cos \phi_B$, $c_1 = J_1 \cos \phi_B + 2J_2 \cos^2 \phi_B$, and $c_2 = J_1 \cos \phi_B + 2J_2 \cos 2\phi_B$. The fields H_j^i are $H_1^A = H - H_{K \text{ eff } A} + H_{KA}$, $H_2^A = H + H_{KA}$, $H_1^B = H \cos \phi_B - H_{K \text{ eff } B} + H_{KB} \cos^2(\phi_B - \delta)$, and $H_2^B = H \cos \phi_B + H_{KB} \cos 2(\phi_B - \delta)$. Finally, $H_{K \text{ eff } A} = 2K_{u \text{ eff } A} / M_A$ ($H_{K \text{ eff } B} = 2K_{u \text{ eff } B} / M_B$) and $H_{KA} = 2K_A / M_A$ ($H_{KB} = 2K_B / M_B$) are, respectively, the effective uniaxial and the planar anisotropy fields for layer A (layer B).

The corresponding mode intensities are given by¹³

$$I = \frac{2ab\omega^2(aq+b)^2}{ab\omega^2(aq^2+b) + b\gamma_A^2[qaH_2^A + c_2(q-1)]^2 + a\gamma_B^2[bH_2^B - c_2(q-1)]^2} \quad (11)$$

where

$$q = \frac{\gamma_A^2 c_2 b (aH_1^A + c_1) + \gamma_A \gamma_B c_0 a (bH_2^B + c_2)}{\gamma_A^2 b (aH_1^A + c_1) (aH_2^A + c_2) + \gamma_A \gamma_B c_0 c_2 a - a^2 b \omega^2}.$$

In the following, Eqs. (10) and (11) will be solved in the particular case of the rigid layer model. The dispersion relation and the variation of the resonance frequency and mode intensity with magnetic field will be discussed. As pointed out earlier, it will be assumed that the applied magnetic field is along the x axis, i.e., $\alpha=0$. As the field is decreased, the

magnetization \mathbf{M}_A will be parallel to \mathbf{H} ($\phi_A=0^\circ$), while the magnetization \mathbf{M}_B direction (ϕ_B) will be given by Eq. (3) for an arbitrary δ value, Eqs. (4a)–(4c) for parallel easy axes ($\delta=0^\circ$) or Eqs. (5a)–(5c) for orthogonal easy axes ($\delta=90^\circ$).

Dispersion relations of coupled layer systems have been investigated in different situations.^{17–22} For the present case, typical examples for the dispersion relation of frequency vs applied field H curves are shown in Figs. 1–6, along with the corresponding intensities, for antiferromagnetic coupling ($J_1 < 0$). In Fig. 1, $\delta=90^\circ$ (perpendicular anisotropy axes),

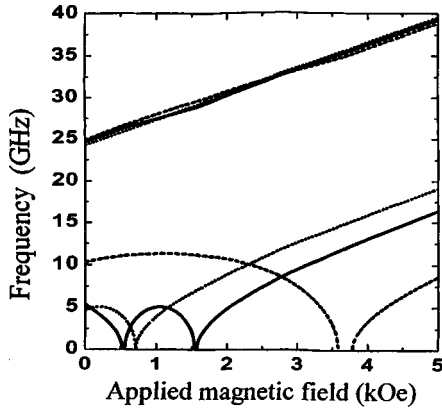


FIG. 1. Resonant frequency vs applied magnetic field H . $\delta = 90^\circ$ (orthogonal anisotropy axes). Solid line, $J_1 = -0.5 \text{ erg/cm}^2$, $J_2 = 0$; dashed line, $J_1 = -0.5 \text{ erg/cm}^2$, $J_2 = -0.5 \text{ erg/cm}^2$; dotted line $J_1 = -0.1 \text{ erg/cm}^2$, $J_2 = 0$. Layer A, $4\pi M_A = 10 \text{ kG}$, $H_{K \text{ eff } A} = -10 \text{ kOe}$, $H_{KA} = 5 \text{ kOe}$, $\gamma/2\pi = 2.8 \text{ GHz/kOe}$, $t = 500 \text{ \AA}$; layer B $4\pi M_B = 6 \text{ kG}$, $H_{K \text{ eff } B} = -6 \text{ kOe}$, $H_{KB} = 0.5 \text{ kOe}$, $\gamma/2\pi = 2.8 \text{ GHz/kOe}$, $t = 100 \text{ \AA}$.

the two branches of the dispersion curves are displayed: the higher-frequency mode is the acoustic mode, while the lower is the optical mode. Different coupling strength parameters are used: $J_1 = -0.5 \text{ erg/cm}^2$, $J_2 = 0$ (solid line), $J_1 = -0.5 \text{ erg/cm}^2$, $J_2 = -0.5 \text{ erg/cm}^2$ (dashed line), and $J_1 = -0.1 \text{ erg/cm}^2$, $J_2 = 0$ (dotted line). For the parameters used in the computation, see the caption of Fig. 1. For the first case, H_{crit} and H_{sat} are, respectively, 0.547 and 1.547 kOe; three regions are considered. For $H < H_{\text{crit}}$, $\phi_B = 180^\circ$, the two magnetizations are antiparallel. For the second region, $H_{\text{crit}} < H < H_{\text{sat}}$, ϕ_B is given by Eq. (5b), and the magnetization \mathbf{M}_B smoothly rotates from the antiparallel configuration ($\phi_B = 180^\circ$) to the parallel one ($\phi_B = 0^\circ$). Finally, for $H > H_{\text{sat}}$, the magnetizations are parallel (ϕ_B

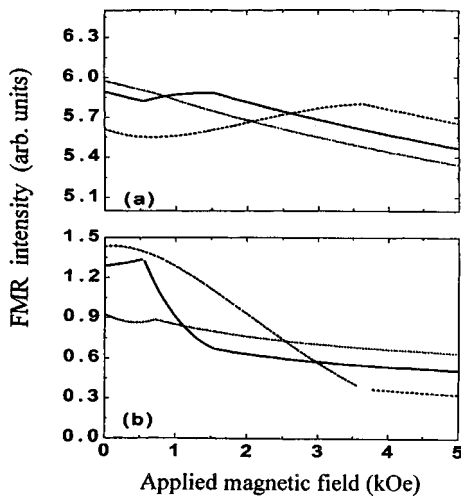


FIG. 2. FMR intensity vs applied magnetic field H . $\delta = 90^\circ$ (orthogonal anisotropy axes). (a) Acoustic and (b) optical modes. Solid line, $J_1 = -0.5 \text{ erg/cm}^2$, $J_2 = 0$; dashed line, $J_1 = -0.5 \text{ erg/cm}^2$, $J_2 = -0.5 \text{ erg/cm}^2$; dotted line, $J_1 = -0.1 \text{ erg/cm}^2$, $J_2 = 0$. Other parameters as for Fig. 1.

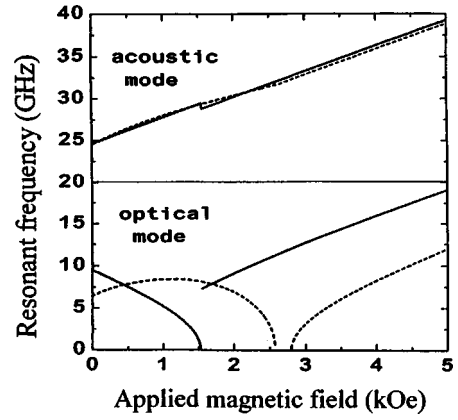


FIG. 3. Resonant frequency vs applied magnetic field H . $\delta = 0^\circ$ (parallel anisotropy axes). Solid line, $J_1 = -0.5 \text{ erg/cm}^2$, $J_2 = 0$; dashed line, $J_1 = -0.5 \text{ erg/cm}^2$, $J_2 = -0.5 \text{ erg/cm}^2$. Other parameters as for Fig. 1.

$= 0^\circ$). Note that the acoustic mode frequency increases in a continuous manner and almost linearly with increasing H ; while the optical mode frequency vs H curve has a more complex variation. As H increases, the frequency decreases to zero at $H = H_{\text{crit}}$ in the first region; then as \mathbf{M}_B rotates the frequency goes through a maximum to go to zero again at $H = H_{\text{sat}}$; for higher field, the frequency monotonically increases with H (see Fig. 1, lower curves). It is easy to check that the fields corresponding to $\omega = 0$ (the zero-frequency points in Fig. 1) are indeed H_{crit} and H_{sat} . Setting $\omega = 0$ in Eq. (10) and solving for H , one will find

$$H(\omega=0) = - \frac{J_1 \cos \phi_B + 2J_2 \cos 2\phi_B}{t_B M_B \cos \phi_B} - \frac{H_{KB} \cos 2(\phi_B - \delta)}{\cos \phi_B}. \quad (12)$$

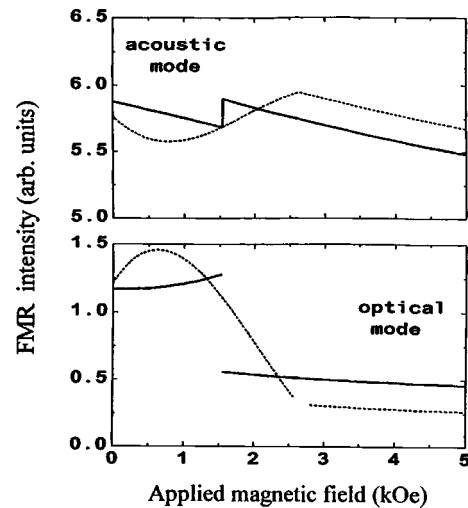


FIG. 4. FMR intensity vs applied magnetic field H . $\delta = 0^\circ$ (parallel anisotropy axes). Solid line, $J_1 = -0.5 \text{ erg/cm}^2$, $J_2 = 0$; dashed line, $J_1 = -0.5 \text{ erg/cm}^2$, $J_2 = -0.5 \text{ erg/cm}^2$. Other parameters as for Fig. 1.

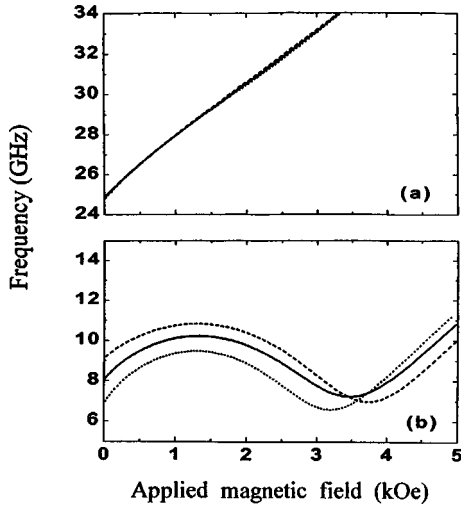


FIG. 5. Resonant frequency vs applied magnetic field H . $J_1 = -0.5$ erg/cm², $J_2 = -0.5$ erg/cm². $\delta = 30^\circ$ (dotted line), 45° (solid line), and 60° (dashed line). Other parameters as for Fig. 1.

For $\phi_B = 180^\circ$, $H(\omega=0)$ [in Eq. (12)] reduces to the critical field [Eq. (7)], and for $\phi_B = 0^\circ$, $H(\omega=0)$ leads to the saturation field [Eq. (6)].

For the situations where $J_1 = -0.5$ erg/cm², $J_2 = -0.5$ erg/cm² and $J_1 = -0.1$ erg/cm², $J_2 = 0$, see the dashed and dotted lines, respectively, in Fig. 1. Here, only two regions exist; the two magnetizations cannot be antiparallel. \mathbf{M}_B will rotate from a certain direction to $\phi_B = 0^\circ$ (saturation). It can be shown that the antiparallel alignment occurs if the effective coupling parameter $J_{\text{eff}} = (J_1 - 2J_2)$ satisfies the condition

$$(J_1 - 2J_2) < t_B M_B H_{KB} \cos 2\delta. \quad (13)$$

The variation of the frequency with field is shown in Fig. 1 (dashed and dotted lines). Note that, in addition to the re-

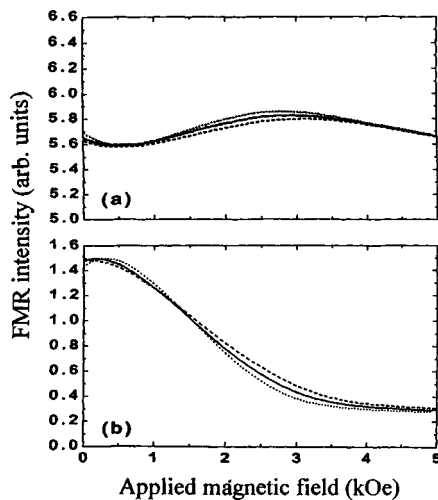


FIG. 6. FMR intensity vs applied magnetic field H . (a) High- and (b) low-frequency modes. $J_1 = -0.5$ erg/cm², $J_2 = -0.5$ erg/cm². $\delta = 30^\circ$ (dotted line), 45° (solid line), and 60° (dashed line). Other parameters as for Fig. 1.

marks made above, the optical mode frequency curve might be discontinuous across the two regions.

The variation of the FMR intensity with H for those cases is shown in Fig. 2. In the saturated state, the intensities of both modes decrease with increasing field for all J_1, J_2 values. On the other hand, in the field region where \mathbf{M}_B rotates, the intensities of the modes have opposite trend; as H increases, the acoustic (optical) mode intensity increases (decreases). When the magnetizations are antiparallel, one also notes opposite variation of the intensities, but in this case, the acoustic mode intensity decreases while the other one increases. Note also that for the acoustic mode the intensities do depend on the J_1, J_2 values [compare the curves in Fig. 2(a)] even though the mode position is practically the same (see Fig. 1, higher curves).

The curves in Fig. 3, drawn for $\delta = 0^\circ$ (parallel easy axes), present some interesting features. Depending on the coupling parameter values, the magnetization \mathbf{M}_B can either smoothly rotate to the direction of \mathbf{H} , or suddenly jump from $\phi_B = 180^\circ$ to $\phi_B = 0^\circ$ as H is increased. Indeed, for $J_1 = -0.5$ erg/cm², $J_2 = 0$ (see solid line in Fig. 3), it is found that H_{crit} is greater than H_{sat} . Therefore when the H value is between H_{sat} and H_{crit} , both $\phi_B = 180^\circ$ and $\phi_B = 0^\circ$ can be solutions of the equilibrium condition. The physical solution will depend on the history of the sample. When H is increased from 0 to a large value, then $\phi_B = 180^\circ$ for low H up to H_{crit} ; at that value, \mathbf{M}_B will suddenly flip, from the 180° to 0° direction, to align with \mathbf{M}_A . [Note that, if one starts for the saturation state (high applied field) and decreases the field, then when $H = H_{\text{sat}}$, \mathbf{M}_B will switch from $\phi_B = 0^\circ$ to $\phi_B = 180^\circ$; and a hysteresis phenomenon can occur. In Fig. 3, only the increasing field case is shown.] One can show that the sudden flip of \mathbf{M}_B occurs (instead of the progressive rotation of \mathbf{M}_B) when

$$J_2 \geq -\frac{1}{2} t_B M_B H_{KB} \cos 2\delta. \quad (14)$$

The solid line in Fig. 3 corresponds to $J_1 = -0.5$ and $J_2 = 0$ erg/cm². With these parameters both Eqs. (13) and (14) are satisfied; thus the antiparallel alignment exists and there will be a sudden flip of \mathbf{M}_B . This sudden flip of \mathbf{M}_B leads to a discontinuity in both branches of the dispersion curves (see the solid line in Fig. 3). Note that the shift to higher frequency (of about 7.3 GHz in the present example) for the optical mode is much more important than the shift to lower value (0.65 GHz) for the acoustic mode. Also, the acoustic mode frequency increases with increasing H in both regions; while for the optical mode the frequency decreases to zero as H increases up to H_{crit} ; then after the discontinuity ($H > H_{\text{crit}}$) the frequency increases almost linearly with H .

The discontinuity in mode position is followed by a discontinuity in the FMR intensity at $H = H_{\text{crit}}$ (Fig. 4). The sudden decrease of the intensity of the optical mode (56.7%) is more important than the increase of the acoustic mode intensity (3.5%). Moreover, in the low field region, the intensity of the optical (acoustic) mode slightly increases (decreases) with H . After the jump ($H > H_{\text{crit}}$) the intensity of both modes decreases. For comparison, the dashed lines in Figs. 3 and 4 are drawn for $J_1 = -0.5$ and $J_2 = -0.5$ erg/cm²; in this situation Eqs. (13) and (14) are not

satisfied, i.e., \mathbf{M}_B will rotate from a given direction at $H=0$ to $\phi_B=0^\circ$ for $H>H_{\text{sat}}$, and there will be no sudden jump of \mathbf{M}_B . In this case, the variation of the mode frequencies with H is qualitatively identical to that found for $\delta=90^\circ$ (compare the dashed curves in Figs. 1 and 3). For the mode intensity (see Fig. 4), in the low-field region ($H<H_{\text{crit}}$), the acoustic (optical) mode intensity decreases (increases), goes through a minimum (maximum), and then increases (decreases); with the variation of the optical mode intensity much more important than the acoustic one. In the saturated state, once again, the intensity of both modes decreases as H increases.

The effect of the B layer easy axis direction, i.e., the angle δ (other than 0° and 90° studied above), on the dispersion relation and on the corresponding intensity is shown in Figs. 5 and 6, respectively. It can be seen that δ has no effect on the resonant frequency of the higher-frequency mode for all H (see Fig. 5, the upper branches); the resonance frequencies monotonically increase with H . On the other hand, for the lower branches (see Fig. 5) δ seems to affect the behavior of this mode. Even though the shapes of the lower curves have similar trends for all δ values (different from 0° and 90°), i.e., the curves present a maximum and a minimum, the values of the frequencies, for a given field, are not the same for all δ . It can be seen from Fig. 5 that for a fixed low field value the resonance frequency of the lower mode increases with increasing δ value; for a high field value, this trend is reversed, i.e., the higher the δ value, the lower the frequency. This difference is even more pronounced for very strong field. Note also that in the f vs H curves the frequency is never equal to zero as was the case for $\delta=0^\circ$ and 90° . In fact, for arbitrary δ , one cannot define H_{crit} and H_{sat} since \mathbf{M}_B will asymptotically tend to $\phi_A=0^\circ$ and $\phi_B=180^\circ$ [$\phi_A=0^\circ$ and $\phi_B=180^\circ$ are not exact solutions for the equilibrium conditions Eqs. 2(a) and 2(b)]. Also, it can be inferred from Fig. 5, as an example, that at the X band, i.e., using a fixed frequency FMR setup at 9 GHz, depending on the δ value, three peaks can be observed for $\delta=45^\circ$ (with different

intensities), two peaks for $\delta=60^\circ$, and only one for $\delta=30^\circ$. As for the mode intensity (see Fig. 6), the lower mode intensity decreases with increasing H for all δ values and the effect of δ is negligible [Fig. 6(b)]. For the higher mode, the intensity curves present a slight variation with H (maximum and minimum in the I vs H curves) and once again the effect of the angle is too small to be experimentally detected [see Fig. 6(a)].

V. CONCLUSION

In the rigid layer model, it is assumed that one of the layers (A) has strong in-plane anisotropy compared to that of the other layer (B) and to the effect of the coupling (J_1, J_2), so that the direction of layer A magnetization (\mathbf{M}_A) is unaffected by the variation of the external field \mathbf{H} applied along its easy axis, while \mathbf{M}_B may rotate. The in-plane anisotropy axes in both layers make an angle δ between them. The dispersion relation of frequency vs H , as well as the variation of the FMR intensity with H of such a system, is studied for different J_1 , J_2 , and δ values. The condition of the antiferromagnetic alignment of the magnetizations at zero field is derived. As the applied field is increased, different switching modes can occur, i.e., \mathbf{M}_B may smoothly rotate or suddenly flip from the antiparallel configuration to the saturated state. A condition for having one or the other case is derived; it involves the biquadratic coupling J_2 and δ . For a sudden switch, a discontinuity is observed in the mode position as well as in the FMR intensity. The discontinuities are more important for the optical than for the acoustic modes. Also, a hysteresis phenomenon can be observed in this case. Moreover, the coupling strengths (J_1, J_2) affect the mode intensity but practically not the position of the acoustic mode; while for the optical mode, the effect of these parameters on the f vs H and I vs H curves is more apparent. Also, for all δ angles (other than 0 and 90°), no effect of δ is observed on the position and intensity of the high-frequency mode but δ does affect the lower-frequency mode position.

-
- ¹P. Grünberg, Acta Mater. **48**, 239 (2000), and references therein.
²J. F. Cochran, J. Rudd, W. B. Muir, B. Heinrich, and Z. Celinski, Phys. Rev. B **42**, 508 (1990).
³J. F. Cochran, J. Magn. Magn. Mater. **169**, 1 (1997).
⁴B. Heinrich, J. F. Cochran, T. Monchesky, and R. Urban, Phys. Rev. B **59**, 14 520 (1999).
⁵J. C. Slonczewski, J. Magn. Magn. Mater. **150**, 13 (1995).
⁶M. E. Filipkowski, C. J. Gutierrez, J. J. Krebs, and G. A. Prinz, J. Appl. Phys. **73**, 5963 (1993).
⁷M. D. Stiles, J. Magn. Magn. Mater. **200**, 322 (1999).
⁸S. M. Rezende, C. Chesman, M. A. Lucena, A. Azevedo, F. M. de Aguiar, and S. S. P. Parkin, J. Appl. Phys. **85**, 5892 (1999).
⁹C. Chesman, M. A. Lucena, M. C. de Moura, A. Azevedo, F. M. de Aguiar, S. M. Rezende, and S. S. P. Parkin, Phys. Rev. B **58**, 101 (1998).
¹⁰T. L. Monchesky, B. Heinrich, R. Urban, K. Myrtle, M. Klaua, and J. Kirchner, Phys. Rev. B **60**, 10 242 (1999).
¹¹H. J. Elmers, G. Liu, H. Fritzsche, and U. Gradmann, Phys. Rev. B **52**, R696 (1995).
¹²B. Heinrich and J. F. Cochran, Adv. Phys. **42**, 523 (1993).
¹³A. Layadi, Phys. Rev. B **65**, 104422 (2002).
¹⁴A. Layadi, J. Magn. Magn. Mater. **266**, 282 (2003).
¹⁵B. Heinrich, Can. J. Phys. **78**, 161 (2000).
¹⁶A. Layadi, Phys. Rev. B **63**, 174410 (2001).
¹⁷A. Layadi, J. Appl. Phys. **83**, 3738 (1998); **85**, 7483(E) (1999).
¹⁸S. M. Rezende, C. Chesman, M. A. Lucena, A. Azevedo, F. M. de Aguiar, and S. S. P. Parkin, J. Appl. Phys. **84**, 958 (1998).
¹⁹Z. Zhang, L. Zhou, P. E. Wigen, and K. Ounadjela, Phys. Rev. B **50**, 6094 (1994).
²⁰S. M. Rezende, C. Chesman, M. A. Lucena, A. Azevedo, F. M. de Aguiar, and S. S. P. Parkin, J. Magn. Magn. Mater. **177-181**, 1213 (1998).
²¹B. Heinrich, M. Kowalewski, and J. F. Cochran, Can. J. Chem. **76**, 1595 (1998).
²²J. Geshev, L. G. Pereira, and J. E. Schmidth, Physica B **320**, 169 (2002).